TECHNICAL PAPER

Electrical and dielectric characterization of a biological liquid using an interdigitated microelectrodes

Meriem Dekmous[1] · Nasreddine Mekkakia-Maaza[1] · Hassan Mouhadjer[1] · Abdelghani Lakhdari[1]

Abstract

In this work, we propose a geometrical analysis of a biosensor with microelectrodes of interdigitated structures, based on the method of impedance spectroscopy in the frequency range below Giga Hertz, to perform an electrical and dielectric characterization of the biological liquid. These characteristics are very important for understanding the cells metabolism that takes place inside the human body. New geometrical relationships are presented, contributing to a new analysis, based on an equivalent electrical model, which according to an optimization study, led us to choose a rectangular shape on the surface of the microsensor. Solutions are proposed to reduce the noise related to the low frequency interface effect in the impedance signal. A comparative study is presented in order to specify the dielectric behavior of human blood from the frequency response of its electrical conductivity and permittivity. MATLAB-Simulink software was used in our case study to simulate the proposed model.

1 Introduction

Determination of the electrical properties and the behavior of a biological medium in lower frequencies than the Giga Hertz are important to do a biomedical diagnostic. This requires an analysis of the electrical bioimpedance of a medium within the biosensor with polarized electrodes which produce an electric field; this technique is called impedance spectroscopy.

In the analytical method, bioimpedance is obtained by modeling the biosensor and the biological medium using an equivalent electrical circuit, which can be represented by a complex bio impedance (a set of resistances and capacities), or even simple which includes only capacities, that depends on the type of sensor used and the desired application; for example, a square shape sensor with two electrodes, one for detection and the other for reference, is applied to the measurement of the bio impedance of a cell culture in real time (Daza et al. 2012).

The characterization of bioimpedances with capacities of interdigitated sensors applied to multilayer structures, generally uses the mapping method to make a modeling (Blume et al. 2015b), to determine the potential and the electric field (Dias & Igreja, 2017), to extract the capacity of a single layer (Shenouda and Oliver 2015). The capacity also contributes to the calculation of the permittivity which can be useful for the detection of humidity (Liang et al. 2018).

The physical and chemical characteristics of biological environments require their modeling by means of a resistance and a capacitance which represent the conductive properties and the dielectric effect respectively.

The medium equivalent circuit has been represented under several models, the most dominant are proposed by Fricke (Fricke and Morse 1926), Cole (Cole 1928) and Debye (Sagor et al. 2013).

Interdigitated electrode sensors are widely used in the biological field, due to their easy-to-use and low cost. Their interaction with a biological medium provides a double layer capacitance. Several researches have optimized this kind of sensor through an equivalent electrical circuit. The purpose is to apply an impedance to detect foodborne pathogenic bacteria (Yang and Bashir 2008), and Esherichia coli (Mejri 2014). Most recent and interesting researches present an interdigitated electrode biosensor sensitive to the DNA molecules used for, the characterization of West Nile virus (Kunjin Strain) (Wang et al. 2017), the detection of avian

✉ Meriem Dekmous
dekmous_meriem@outlook.com;
meriem.dekmous@univ-usto.dz

1 LMSE, Microsystems and Embedded Systems Laboratory, University of Science and Technology of Oran Mohamed Boudiaf, BP1505 El Mnaouer, 31000 Oran, Algeria
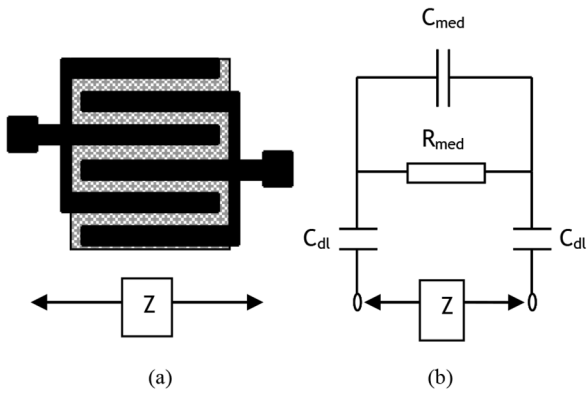
Fig. 1 **(a)** Intédigitated sensor in presence of a biological fluid. **(b)** The equivalent elctrical circuit

influenza virus from foodborne pathogens and the detection of pesticide residues based on impedance sensing for different virus concentrations (Wang et al. 2015).

One of the main problems encountered in modeling is the significant effect of the double layer capacitance on the measured and calculated impedance, because its response has a wide frequency bandwidth, resulting in a bad reading of the electrical and dielectric response of the biological medium. In this case, we have optimized the geometrical parameters of a sensor with interdigitated microelectrodes, in order to minimize the effect of the double layer capacitance, and to carry out a study of the conductivity and permittivity of the biological medium in order to understand its electrical aspect.

2 Method for determination of sensor parameters

Fig. 1(a), shows a sensor model based on an interdigitated electrode structure mounted on an insulating material substrate. The presence of a biological liquid on this sensor produces a Z impedance when the system is supplied with energy source. The Z impedance is represented by electrical components in the equivalent electrical circuit as shown in Fig. 1(b).

2.1 Optimization of the equivalent circuit (biological medium + sensor)

The circuit model of Fig. 1 (b) has been developed by several works (Hong et al. 2005; Linderholm et al. 2004), in which the resistor R_{med} and the capacitor C_{med}, modelling respectively the electrical and dielectric phenomena of the biological environment under the influence of the electric field (Ibrahim et al. 2013), were been taken based on the Fricke model (Fricke et al., 1926) which described

biological cells by a plasma membrane capacitor in series with an intracellular resistor, and in parallel with a resistor representing the extracellular liquid.

In our study, the intracellular resistance is considered negligible because according to Fricke's model, it only appears in circuits that operate at very high frequencies, and our circuit operates in lower frequencies.

The interaction of the biological medium with the sensor electrodes produces two capacities called double layer capacitances C_{dl}, given by Eq. (1):

$$C_{dl} = A.C_{dla} = W.L.\frac{N}{2}.C_{dla} \qquad (1)$$

Where A is the surface of the electrodes inserted at the positive or negative pole, W is the width of electrode [µm], L is the length of an electrode [µm] and N is the number of electrodes.

C_{dla} is the characteristic capacitance which represents the capacitance per unit area [pF/µm2] of the double layer, it is a function of, the permittivity of the vacuum: ϵ_0 = 8,85. 10^{-12} [F/m²], the relative permittivity of the double-layer zone ϵ_{dl} and the characteristic thickness of the double layer d [µm], Eq. (2):

$$C_{dla} = \frac{\epsilon_0.\epsilon_{dl}}{d} \qquad (2)$$

In the model of Fig. 2, we replace the two capacities C_{dl} of Fig. 1 (b) by a single total capacity C_{dlT} as represented in Eq. (3):

$$C_{dlT} = \frac{C_{dl}}{2} = \frac{1}{4}W.L.N.C_{dla} \qquad (3)$$

Therefore, the two double layer capacitances C_{dl} in Fig. 1 (b) will be modeled by a single capacitance C_{dlT}. The resulting equivalent electrical circuit shown in Fig. 2, will be modeled by a resistance of the biological medium R_{med} in parallel with its capacitance C_{med}, and the whole in series with the equivalent double layer capacitance C_{dlT}.

2.2 Electrical circuit parameters determination

The equivalent electrical impedance Z will be calculated from the circuit of Fig. 2 as given in Eq. (4):

$$Z = \frac{R_{med}}{1 + j.R_{med}.C_{med}.\omega} + \frac{1}{j.C_{dlT}.\omega} \qquad (4)$$

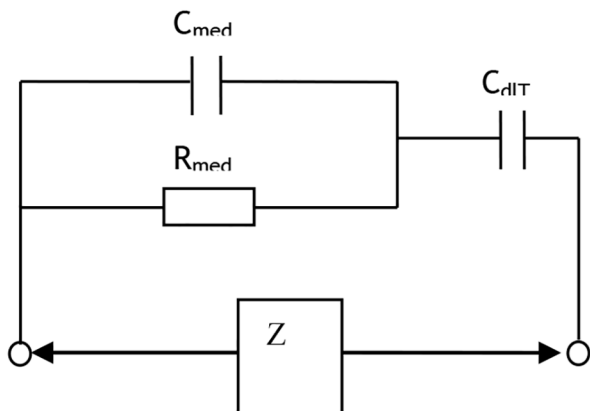Where the angular pulsation ω [rad / s] is related to the frequency f [Hz]: ω = 2πf. j is an imaginary number.

Fig. 2 The model of the equivalent electrical circuit

The resistance of the biological medium Rmed depends essentially on the conductivity of this medium σ (S / m), as well as the cell constant Kcell (m^{-1}) (Olthuis et al. 1995), and is given by the Eq. (5):

$$R_{med} = \frac{K_{cell}}{\sigma} \tag{5}$$

According to Eq. (6), the capacity of the biological medium Cmed also depends on the cell constant Kcell, as well as the relative permittivity of the medium and the permittivity of vacuum $\epsilon_0 = 8,85.\,10^{-12}$ [F/m^2] (Ibrahim et al. 2013):

$$C_{med} = \frac{\epsilon_0.\epsilon r_{med}}{K_{cell}} \tag{6}$$

Equations (7), (8) and (9) show the relationship of the cell constant Kcell to the sensor geometry, where S indicates the electrode gap [μm].

$$K_{cell} = \frac{2.K\,(k)}{(N-1)\,.L.K(\sqrt{1-k^2})} \tag{7}$$

$$K\,(k) = \int_0^1 [(1-t^2)\,.(1-k^2t^2)]^{-\frac{1}{2}}.dt \tag{8}$$

$$k = cos\left(\frac{\pi.W}{2.\,(W+S)}\right) \tag{9}$$

In another way, the total double-layer capacity depends on the constant Kcell and the permittivity of the vacuum and the relative permittivity as shown in Eq. (10), according to the homogeneous and isotropic dielectric medium (Bard and Faulkner 2002; Olthuis et al. 1995):

$$C_{dlT} = \frac{\epsilon_0.\epsilon_r}{K_{cell}} \tag{10}$$

This relative permittivity or so-called dielectric constant of the blood is equal to 5300 in the low frequency band and 60 in the high frequency band (Aufray et al. 2012).

By equalizing Eq. (3) with Eq. (10), we can deduce the expression of Cdla represented by Eq. (11).

$$C_{dla} = \frac{4.\epsilon_0.\epsilon_r}{K_{cell}.W.L.N} \tag{11}$$

2.3 Geometric analysis for the structures choice

Due to the reduction of interface effects that occur by the interaction between sensor and biological medium, occupying a wide frequency band in the frequency response of the impedance and overlapping with the useful frequency band (frequency band that characterizes the biological medium), we can use the expression of the low cutoff frequency to make our choice of structures, given in Eq. (12);

$$f_{lo} = \frac{1}{2.\pi.R_{med}.C_{dlT}} \tag{12}$$

By replacing the expressions; Eq. (3), Eq. (5) and Eq. (7) in the Eq. (12), we obtain the Eq. (13):

$$f_{lo} = \frac{\sigma.\,(N-1)\,.K(\sqrt{1-k^2})}{\pi.W.N.C_{dla}.K\,(k)} \tag{13}$$

To simplify our optimization, we will introduce two ratios: Mr and Sr given in Eq. (14) and Eq. (15) respectivelly:

$$M_r = \frac{S}{W} \tag{14}$$

$$S_r = \frac{(W+S)\,.N}{L} \tag{15}$$

Where:

Mr: The ratio between the width and the spacing between the two electrodes (metallization ratio).

Sr: The ratio between the total width and the length of the sensor (surface ratio of the sensor).

By replacing the two equations; Eq. (14) and Eq. (15) in Eq. (13), the expression of the low cutoff frequency Flo becomes as in the following Eq. (16):

$$f_{lo} = \frac{\sigma.\,(N-1)\,.K(\sqrt{1-k^2})}{\pi.L.Cdla.\left(\frac{S_r}{M_r+1}\right).K\,(k)} \tag{16}$$
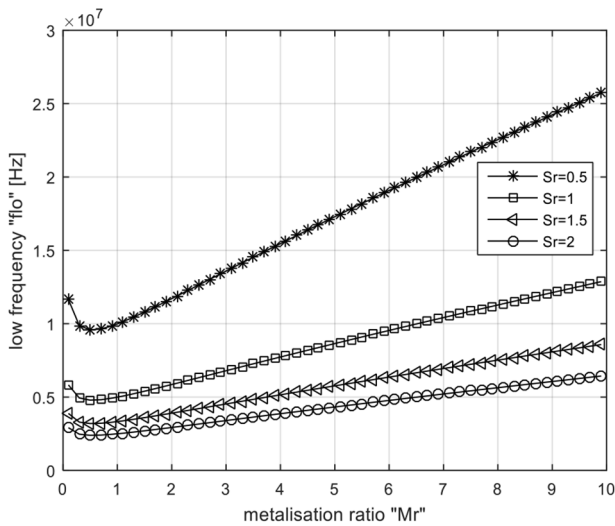
Fig. 3 The low cutoff frequency according to the metallization ratio for different surface ratio values of the sensor
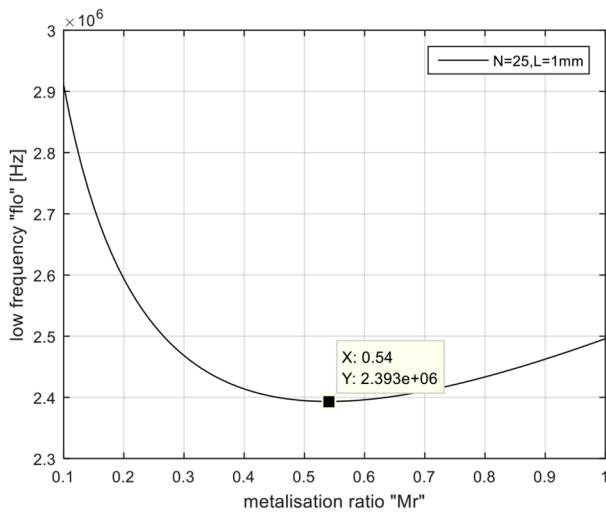
Fig. 4 The low cutoff frequency according to the metallization ratio for Sr = 2

The optimization of the geometric structures of the sensor is obtained from an analysis of the low cut-off frequency. Indeed, Eq. (16) will be used to define the two ratios Sr and Mr which is used to determine the best geometrical structures of our sensor, taking into account: N = 25, L = 1000 μm.

Fig. 3 and Fig. 4 show the variation of the low cut-off frequency lo for different values of the Sr and Mr ratios.

The result of Fig. 3 shows that we have to choose a surface ratio Sr = 2, to have the lowest value of the low cut-off frequency flo, in this case the sensor have a rectangular shape. Thus, we observe that the metallization ratio must be less than 1 (Mr < 1) or the electrode width W is greater than the spacing S, for the low cut-off frequency to pass through

its minimum values. And in order to determine the optimal value of the metallization ratio, we have swept the latter between 0.1 and 1 as shown in Fig. 4, and by consequence, the obtained metallization ratio Mr is about 0.54.

Using this geometric analysis and simulation we obtained optimized values represented in Table 1:

2.4 Electrical and dielectrical parameters of biological medium

The relative permittivity of the biological medium is obtained from the expression of the impedance Z (Eq. 4), which is given by Eq. (17)

$$\epsilon_r = \frac{imag\left(\frac{K_{cell}}{Z}\right)}{\epsilon_0 . \omega} \tag{17}$$

Generally, biological medium do not have a very high conductivity (Tarasov and Titov 2013), represented by Eq. (18): flo$_4$

$$\sigma = \sigma_\infty + \frac{\sigma_0 - \sigma_\infty}{1 + (\omega\tau)^2} \tag{18}$$

Where: σ_∞, σ_0 are the conductivities in high and low frequencies respectively, τ is the relaxation time.

3 Results and discussion

In order to study the effect of the metallization ratio and the area ratio on the low cut-off frequency, we visualized the frequency response of the impedance as shown in the Figs. 5 and 6 for different values of the two ratios and thus different sensor geometries. These values are shown in Table 2, taking into account that the value of the number of electrodes and the length of an electrode are constant in all cases: N = 35 and L = 1000 μm.

Because of the overlap between the five curves obtained in the high frequencies as shown in Fig. 5, we made a zoom in the frequency range of [10^6 – 10^7 Hz] as shown in Fig. 6 ; the goal is to extract the low cut-off frequency for each curve corresponding to the different geometries.
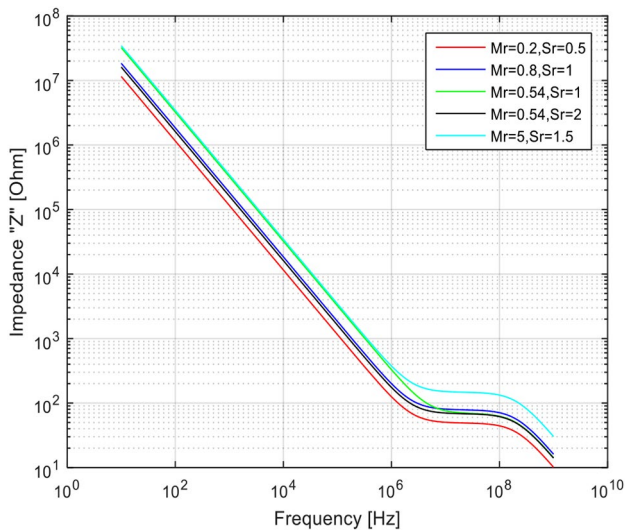
The frequency response of the impedance in Fig. 5 is divided into three zones, corresponding to the three components of the equivalent electrical circuit in Fig. 1.

The first interval below the low cut-off frequency represents the discharge of the C$_{dlT}$ capacitance, because the effect of Cmed is negligible compared to C$_{dlT}$ in this case.

The second interval between the low and high cut-off frequencies, the curve is constant which is represents the impedance Rmed.
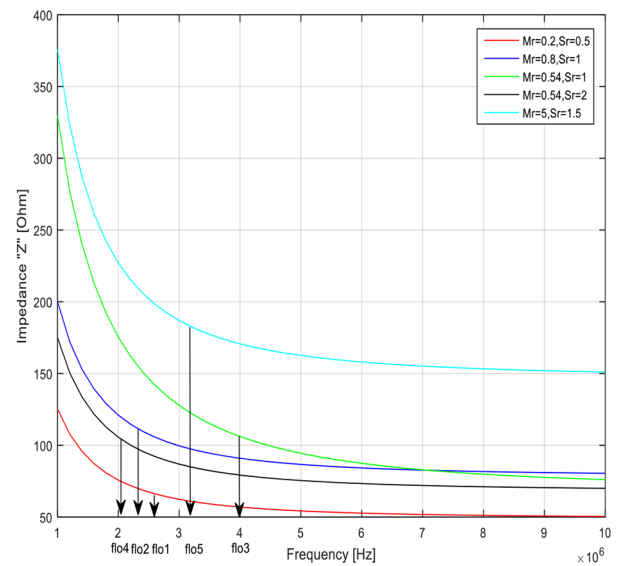
Table 1 Parameters of equivalent electrical circuit

	N	W [μm]	K_{cell} [m^{-1}]	R_{med} [Ω]	C_{med} [pF]	C_{dlT} [pF]	C_{dla} [pF/μm^2]
(1)	5	259.74	401.50	573.5765	1.32	115.94	3.57×10^{-4}
(2)	10	129.87	178.44	254.9228	2.97	260.87	8.03×10^{-4}
(3)	15	86.58	114.71	163.8790	4.62	405.81	1.25×10^{-3}
(4)	20	64.93	84.52	120.7530	6.28	550.71	1.69×10^{-3}
(5)	25	51.94	66.91	95.5961	7.93	695.64	2.14×10^{-3}
(6)	30	43.29	55.37	79.1140	9.58	840.58	2.59×10^{-3}
(7)	35	37.10	47.23	67.4795	11.24	985.51	3.03×10^{-3}
(8)	40	32.46	41.18	58.8284	12.89	1130.42	3.48×10^{-3}
(9)	45	28.86	36.50	52.1432	14.54	1275.35	3.92×10^{-3}
(10)	50	25.97	32.77	46.8225	16.20	1420.29	4.37×10^{-3}
(11)	55	23.61	29.74	42.4871	17.85	1565.22	4.82×10^{-3}
(12)	60	21.64	27.22	38.8865	19.50	1710.12	5.26×10^{-3}
(13)	65	19.98	25.09	35.8485	21.16	1855.06	5.71×10^{-3}
(14)	70	18.55	23.27	33.2508	22.81	1999.99	6.16×10^{-3}
(15)	75	17.31	21.70	31.0041	24.46	2144.93	6.60×10^{-3}
(16)	80	16.23	20.32	29.0419	26.12	2289.86	7.05×10^{-3}

Fig. 5 Impedance frequency response

Fig. 6 Impedance frequency response in [10^6- 10^7 Hz]range

At the third and last interval above the high cut-off frequency, the curve is slightly decreasing, corresponding to the discharge of the Cmed capacitance.

The sensor parameters listed in Table II and shown in Figs. 5 and 6 confirm that the optimal values of the metallization ratio and the surface ratio are Mr = 0.54 and Sr = 2 respectively, and therefore the sensor number (4) gave the lowest value of the low cutoff frequency flo4 = 2.01 MHz, as well as the lowest value of the capacitance Cdla = 3.06 × 10^{-3} [pF/μm^2], which minimizes the interface effects that occur at the electrode-electrolyte interface, which confirms our approach.

Table 2 Parameters of different sensor geometries

The sensor number	Mr	Sr	W [μm]	S [μm]	C_{dla} [pF/μm^2]	f_{lo} [MHz]
(1)	0.2	0.5	11.9	2.38	13.25×10^{-3}	2.49
(2)	0.8	1	15.87	12.69	6.22×10^{-3}	2.24
(3)	0.54	1	18.55	10.02	6.11×10^{-3}	4
(4)	0.54	2	37.10	20.04	3.06×10^{-3}	2.01
(5)	5	1.5	7.14	35.71	7.36×10^{-3}	3.37
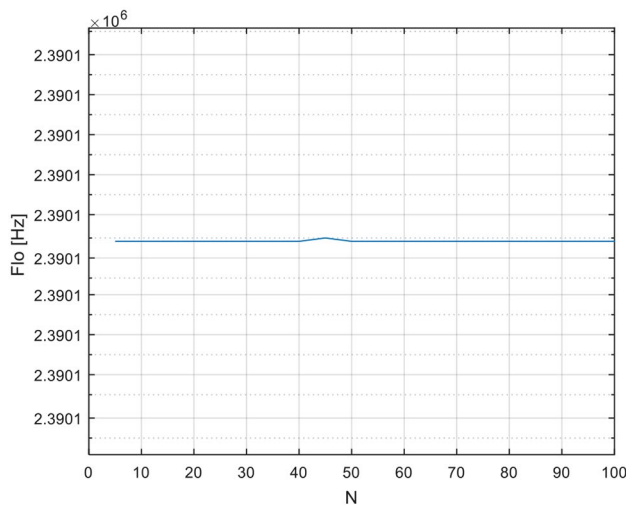
Fig. 7 The variation of low cutoff frequency vs. the number of electrodes

In order to select a structure from the Table I and to simulate the physical properties of the biological environment, it is necessary to consider the influence of the electrodes number N on the low cut-off frequency flo, taking into account that all the structures indicated in Table I have the same contact surface mentioned in Eq. (19):

$$Ac = W.L.N = 12.98 \times 10^5 \mu m^2 \qquad (19)$$

Fig. 7 shows the variation of low cutoff frequency flo as a function of the number of electrodes N:

We Note from Fig. 3 that the effect of the number of electrodes on the low cutoff frequency is negligible, this is almost in agreement with Eq. (13): for $N \geq 5$ electrodes, $\frac{N-1}{N} \cong 1$; On the other hand, if $N < 5$ the value of the low cut-off frequency will be approximately halved because $\frac{N-1}{N} \cong 0,5$; this is useful for our optimization but on the other hand affects the sensitivity of impedance measurement, the cell constant K increases and the variations in impedance generated by our sensor are difficult to detect. For this reason, we study the sensitivity of the cell constant K with regard to the electrodes numbers N as shown in Eq. (20):

$$S = \left| \frac{\Delta K}{\Delta N} \right| \qquad (20)$$

Table 3 shows the values of the variation sensitivity of the Kcell constant with regard to the variation of the electrodes number:

The value of the cell constant is inversely proportional to the number of electrodes, this result is shown in the Table 3 by (Ngo et al. 2016) and confirmed by (Blume et al. 2015a) who indirectly found that the increase in the electrodes

Table 3 Evaluation of sensitivity

The authors	N 1	N 2	K 1 [m^{-1}]	K 2 [m^{-1}]	Sensitivity [m^{-1}]
(Ngo et al. 2016)	10	14	94.45	65.39	7.26
	36	40	24.29	21.80	0.62
	46	50	18.89	17.35	0.38
Our results	10	15	178.44	114.71	12.74
	35	40	47.23	41.18	1.21
	45	50	36.50	32.77	0.74
	55	60	29.74	27.22	0.50
	75	80	21.70	20.33	0.27

number N and the decrease in the width electrode width W leads to the decrease in the cell constant K.

Table 3 shows that sensitivity gradually decreases with increasing of electrodes number, which is close to the values obtained by (Ngo et al. 2016).

The value of the sensitivity is ten times higher if less than 15 electrodes are used, which means that the cell constant K is not really constant. On the other hand, if the number of electrodes is increased to more than 35, the sensitivity value becomes less than or equal to 1, and therefore the change in the Kcell constant becomes negligible. Indeed, for a better optimization, it is better to take structures with more than 35 electrodes.

These results are in good agreement with those of (Bourjilat et al. 2018) who optimized a sensor with a metallization ratio Mr = 0.5, and a number of electrodes N = 80.

Finally, we studied the variation of permittivity εr as a function of frequency as shown in Fig. 8. Table 4 shows the comparative values of the double layer parameters obtained in our study and the results obtained by (Borkholder 1998), (Wolf et al. 2011) and (Gun 2017).

In Fig. 8, the relative permittivity curve obtained is similar to all other curves from previous work and closer to the (Wolf et al. 2011) curve. The permittivity of blood is about 5260 in the low frequencies and 60 in the high frequencies, which is in agreement with the results obtained by (Aufray et al. 2012). Thus we notice that in the high frequencies the relative permittivity of blood is between 40 and 80, which is in agreement with the experimental results obtained by (Ley et al. 2019).

The optimization of the sensor is essentially based on the study of the frequency response of the electrical conductivity shown in Fig. 9. Table 5 presents this parameter for previous results of (Ma and Ea 2014), (Wolf et al. 2011), (Abdalla 2011), as well as the results obtained by our model:

Two relaxation time values in Table 5 are very close to our value, that of (Abdalla 2011) and (Wolf et al. 2011).

(Wolf et al. 2011) has experimentally studied the dielectric properties of human blood in its different regions of dispersion by varying the temperature. We have simulated the dispersion region β as it fits with our studied frequency range, and we took the result for a temperature of 288 °K.
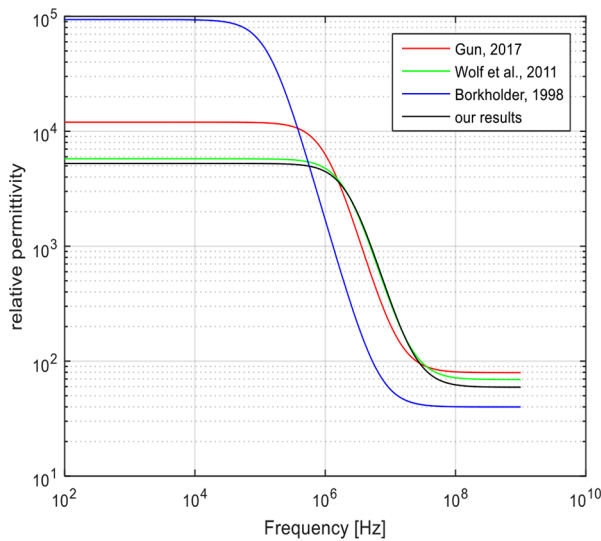
Fig. 8 Relative permittivity of human blood variation vs. frequency

Table 4 Dielectric properties of the system

Les auteurs	C_{dla} [pF/µm²]	ϵ_{dl}
(Borkholder 1998)	70×10^{-3}	7906
(Wolf et al. 2011)	4.3×10^{-3}	486.27
(Gun 2017)	8.96×10^{-3}	1012.6
Our results	3.92×10^{-3}	442.93
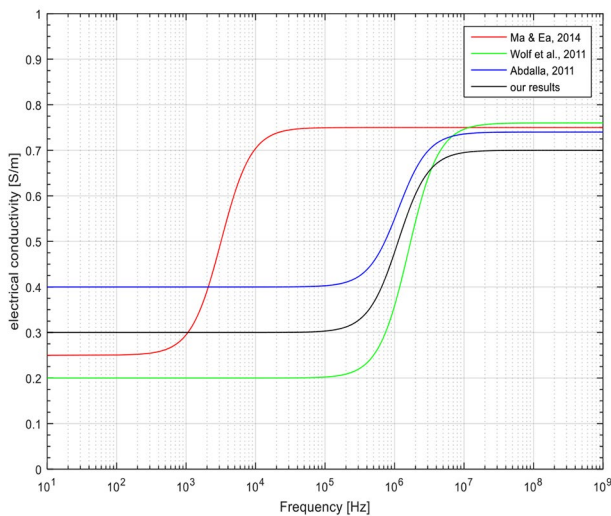
Fig. 9 Electrical conductivity of human blood variation as a fonction of frequency

Table 5 Relaxation time for different authors

Authors	Relaxation time $\tau = RC$ [s]
(Ma and Ea 2014)	$5.\,10^{-5}$
(Wolf et al. 2011)	$0{,}89.\,10^{-7}$
(Abdalla 2011)	$1{,}41.\,10^{-7}$
Our results	$0{,}66.\,10^{-7}$

(Abdalla 2011) studied the frequency variation of conductivity for different glucose rates in human blood, the representation of their work and the value of the rate were taken for a glucose concentration equal to 122.3 mg/L.

Note that (Ma and Ea 2014) in Fig. 9 is slightly different from the other curves. Its conductivity variation appears before the others curves in the frequencies between 10^2 and 10^5 Hz. This is due to the minimum value of the relaxation rate in comparison with Table V. He experimentally analyzed the resistance and electrical capacity of red blood cells, which represent 95% of the blood cytoplasm. Then the relaxation time of the red blood cells is less than the relaxation time of a complete blood sample.

There is not much difference in the variation of conductivity at low and high frequencies, in the case of our curve and those of (Wolf et al. 2011), (Abdalla 2011) and (Ma and Ea 2014). The sensitivity of the conductivity variation is better in the high frequencies because, the conductivity varies around 0.7 S/m to 0.76 S/m, while in the low frequencies it varies between 0.2 S/m and 0.4 S/m, this is due to the polarization phenomenon and the double layer capacitance that occur in the low frequencies and which is different in the obtained four curves.

We also notice a significant increase in conductivity, and in the same time a decrease in relative permittivity mainly in the frequency range from a hundred kHertz to a few tens of MHertz (10^5 Hz – 2.10^7 Hz) Figs. 8 and 9, this is due to the decrease in the value of the membrane capacity of blood cells, which allows the passage of current through the intra and extra cellular medium, thus resulting in an apparent increase in conductivity. This dielectric behavior of biological medium in this frequency range has been named dispersion β by (Schwan 2002), who noted that this dispersion occurs in a relative permittivity range between 50 and 100 at high frequencies and between 10^3 and 10^5 at low frequencies and in a conductivity range between 0.1 S/m and 1 S/m; which is in agreement with our results and with other recent works such as those of (Rivas-Marchena et al. 2017).

4 Conclusion

An interdigitated microelectrode biosensor was used for the electrical and dielectric characterization of human blood at frequencies below the Giga Hertz, using an analytical model of an electrical circuit simulated by Matlab.

A new method of geometric analysis has been developed which led us to choose a rectangular shape on the surface of the studied microsensor. This method allowed us to optimize an area ratio Sr = 2 and a metallization ratio Mr = 0.54. The optimal values of the number of electrodes must be higher than 35 to have a response of the microsensor and to characterize the biological liquid.

A comparative study of the electrical properties of human blood (permittivity and conductivity) has shown that the electrical model of our sensor in the frequency range (0 to 10^9 Hz), is suitable for modeling the electrical behavior of the plasma membrane at the time of ionic exchanges between intra- and extracellular liquids, through the transmembrane channels.

References

Abdalla S (2011) Effect of erythrocytes oscillations on dielectric properties of human diabetic-blood. AIP Adv 1(1). https://doi.org/10.1063/1.3556986

Aufray M, Brochier A, Possart W (2012) Interval analysis applied to dielectric spectroscopy: A guaranteed parameter estimation. IFAC Proceedings Volumes (IFAC-PapersOnline), 45(16 PART 1). https://doi.org/10.3182/20120711-3-BE-2027.00308

Bard a, Faulkner L (2002) Electrochemical Methods: Fundamentals and Applications, New York:, 2001.Russian Journal of Electrochemistry, 38(12)

Blume SOP, Ben-Mrad R, Sullivan PE (2015a) Characterization of coplanar electrode structures for microfluidic-based impedance spectroscopy. Sens Actuators B: Chem 218. https://doi.org/10.1016/j.snb.2015.04.106

Blume SOP, Ben-Mrad R, Sullivan PE (2015b) Modelling the capacitance of multi-layer conductor-facing interdigitated electrode structures. Sens Actuators B: Chem 213. https://doi.org/10.1016/j.snb.2015.02.088

Borkholder Da (1998) Cell Based Biosensors using Microelectrodes. PhD Thesis

Bourjilat A, Sarry F, Kourtiche D, Nadi M (2018) Modelization of interdigitated electrode sensor for impedance spectroscopy measurement. Proceedings of the International Conference on Sensing Technology, ICST, 2017-December. https://doi.org/10.1109/ICSensT.2017.8304461

Cole KS (1928) Electric impedance of suspensions of spheres. J Gen Physiol 12(1). https://doi.org/10.1085/jgp.12.1.29

Daza P, Cañete D, Olmo A, García JA, Yúfera A (2012) Cell-culture real time monitoring based on bio-impedance measurements. Sensors and Transducers, 14(SPEC. 1)

Dias CJ, Igreja R, Physical A (2017) 256. https://doi.org/10.1016/j.sna.2017.01.021

Fricke H, Morse S (1926) The electric capacity of tumors of the breast. J Cancer Res 10(3). https://doi.org/10.1158/jcr.1926.340

Gun L (2017) Equivalent Permittivity Based on Debye Model of Blood and Its SAR. Int J Sci Technol Soc 5(3). https://doi.org/10.11648/j.ijsts.20170503.12

Hong J, Yoon DS, Kim SK, Kim TS, Kim S, Pak EY, No K (2005) AC frequency characteristics of coplanar impedance sensors as design parameters. Lab Chip 5(3). https://doi.org/10.1039/b410325d

Ibrahim M, Claudel J, Kourtiche D, Nadi M (2013) Geometric parameters optimization of planar interdigitated electrodes for bioimpedance spectroscopy. J Electr Bioimpedance 4(1). https://doi.org/10.5617/jeb.304

Ley S, Schilling S, Fiser O, Vrba J, Sachs J, Helbig M (2019) Ultrawideband temperature dependent dielectric spectroscopy of porcine tissue and blood in the microwave frequency range. Sens (Switzerland) 19(7). https://doi.org/10.3390/s19071707

Liang JG, Wang C, Yao Z, Liu MQ, Kim HK, Oh JM, Kim NY (2018) Preparation of Ultrasensitive Humidity-Sensing Films by Aerosol Deposition. ACS Appl Mater Interfaces 10(1). https://doi.org/10.1021/acsami.7b14082

Linderholm P, Bertsch A, Renaud P (2004) Resistivity probing of multi-layered tissue phantoms using microelectrodes. Physiol Meas 25(3). https://doi.org/10.1088/0967-3334/25/3/005

Ma K, Ea E (2014) Dielectric Properties of Red Blood Corpuscles of Workers Chronically Exposed To Benzene in Workplace. 10:365–37818

Mejri MB, B. H (2014) Interdigitated Microelectrode Arrays Integrated in Microfluidic Cell for Biosensor Applications. J Nanomed Nanotechnol 05(06). https://doi.org/10.4172/2157-7439.1000243

Ngo TT, Bourjilat A, Claudel J, Kourtiche D, Nadi M (2016) Design and realization of a planar interdigital microsensor for biological medium characterization. In Smart Sensors, Measurement and Instrumentation (Vol. 16). https://doi.org/10.1007/978-3-319-21671-3_2

Olthuis W, Streekstra W, Bergveld P (1995) Theoretical and experimental determination of cell constants of planar-interdigitated electrolyte conductivity sensors. Sens Actuators: B Chem 24(1–3). https://doi.org/10.1016/0925-4005(95)85053-8

Rivas-Marchena D, Olmo A, Miguel JA, Martínez M, Huertas G, Yúfera A (2017) Real-time electrical bioimpedance characterization of neointimal tissue for stent applications. Sens (Switzerland) 17(8). https://doi.org/10.3390/s17081737

Sagor RH, Saber MG, Al-Amin MT, Noor A, Al (2013) An optimization method for parameter extraction of metals using. Modified Debye Model SpringerPlus 2(1). https://doi.org/10.1186/2193-1801-2-426

Schwan HP (2002) Electrical properties of tissues and cell suspensions: mechanisms and models. https://doi.org/10.1109/iembs.1994.412155

Shenouda M, Oliver DR (2015) Fabrication of an interdigitated sample holder for dielectric spectroscopy of thin films. Journal of Physics: Conference Series, 619(1). https://doi.org/10.1088/1742-6596/619/1/012028

Tarasov A, Titov K (2013) On the use of the Cole-Cole equations in spectral induced: Polarization. Geophys J Int 195(1). https://doi.org/10.1093/gji/ggt251

Wang L, Veselinovic M, Yang L, Geiss BJ, Dandy DS, Chen T (2017) A sensitive DNA capacitive biosensor using interdigitated electrodes. Biosens Bioelectron 87. https://doi.org/10.1016/j.bios.2016.09.006

Wang X, Zhao Z, Wang Y, Lin J (2015) A portable impedance detector of interdigitated array microelectrode for rapid detection of avian influenza virus. IFIP Adv Inform Communication Technol 452. https://doi.org/10.1007/978-3-319-19620-6_31

Wolf M, Gulich R, Lunkenheimer P, Loidl A (2011) Broadband dielectric spectroscopy on human blood. Biochim Biophys Acta Gen Subj 1810(8). https://doi.org/10.1016/j.bbagen.2011.05.012

Yang L, Bashir R (2008) Electrical/electrochemical impedance for rapid detection of foodborne pathogenic bacteria. Biotechnol Adv (Vol 26. https://doi.org/10.1016/j.biotechadv.2007.10.003